Vibration Analysis of the Active Multi-Layer Beams by Using Spectrally Formulated Exact Natural Modes

Joohong Kim, Usik Lee*
Department of Mechanical Engineering, Inha University
Andrew Y. T. Leung
Mechanical Engineering Division, Manchester University, UK

Modal analysis method (MAM) is introduced for the fully coupled structural dynamic problems. In this paper, the beam with active constrained layered damping (ACLD) treatment is considered as a representative problem. The ACLD beam consists of a viscoelastic layer that is sandwiched between the base beam structure and an active piezoelectric layer. The exact damped natural modes are spectrally formulated from a set of fully coupled dynamic equations of motion. The orthogonality property of the exact damped natural modes is then derived in a closed form to complete the modal analysis method. The accuracy of the present MAM is evaluated through some illustrative examples: the dynamic characteristics obtained by the present MAM are compared with the results by spectral element method (SEM) and finite element method (FEM). It is numerically proved that MAM solutions become identical to the accurate SEM solutions as the number of exact natural modes used in MAM is increased.

Key Words : Vibration, Spectral Element Method, Active Multi-Layer Beams, Modal Analysis

1. Introduction

During the last decade, piezoelectric materials (simply, PZT) have received considerable attention due to their potential applications to the active controls of structural vibration and noise. The converse piezoelectric effect is used for the actuator design while the direct piezoelectric effect is used for the sensor design. In order to use the piezoelectric effects, the PZT layers are usually bonded on the surfaces of base structures to result in various active multi-layer laminate structures (Crawley and de Luis, 1987). This paper will consider the elastic-VEM-PZT three-layer beam that consists of the elastic base layer, the viscoelastic material (simply, VEM) layer, and the PZT layer. In the literature, this three-layered beam is often called active constraining layer damping treated beam or, simply, ACLD beam (Baz, 1993).

There have been developed diverse structure models for ACLD beams: the analytical models (e.g., Baz, 1993; Liao, 1997), the finite element models (e.g., Robbins and Reddy, 1991; Lesieutre and Lee, 1996), and the spectral element model (Lee and Kim, 1999). Despite of numerous analytical models, some models are not appropriate for practical uses. This is due to the strict assumptions used to derive extremely simplified models or due to the mathematical complexity involved in the analytical models. On the other hand, the finite element method (FEM) has provided more realistic structural models by removing unnecessary strict assumptions. However, as the drawback of FEM, very precise structural discretization is often required to obtain reliable solutions, especially at high frequency. Furthermore, the modal analysis commonly used in conjunction

* Corresponding Author,
E-mail : ulee@dragon.inha.ac.kr
TEL : +82-32-860-7318 ; **FAX** : +82-32-866-1434
Department of Mechanical Engineering, Inha University, 253 Yonghyun-Dong, Nam-Ku, Inchon 402-751, Korea. (Manuscript **Received** June 8, 2000; **Revised** October 16, 2000)

with FEM is limited to the frequency regime where the relative spacing of natural frequencies remains large compared to the relative parameter uncertainty. Thus, as an alternative to FEM, the spectral element method (SEM) has been well proved to overcome some drawbacks of FEM to provide very accurate dynamic characteristics of smart beams (Lee and Kim, 1999, 2000b).

The spectral element method (SEM) was attributed to Doyle (Doyle, 1988) and was applied to various wave propagations in structures (Doyle, 1997) and structural dynamics problems (e.g., Lee, 1998; Lee and Lee, 1999; Lee, 2000; Lee and Kim, 2000a; Lee and Kim, 2000b). In contrast to the finite elements used in conventional FEM, the spectrally formulated finite elements (simply spectral element) used in SEM treat the mass distribution within a structural element exactly by using exact eigenfunctions or shape functions. Thus, SEM provides very accurate dynamic characteristics of a structure and it is often justifiably referred to as an exact method (Banerjee, 1997). Thus, in the authors' previous work (Lee and Kim, 1999), a spectral element model for ACLD beams has been developed directly from fully coupled differential equations of motion.

The modal analysis method (MAM) is very popular in structural dynamics. In the literature, Dokumaci (1987), Bishop *et al.* (1989), Banerjee (1989), and Banerjee *et al.* (1996) have conducted modal analysis for the coupled differential equations of motion. The coupled differential equations of motion considered in their works are the equations all can be combined into a single equation, which made it easy to apply the modal analysis approach. However, it is not always possible to reduce the fully coupled differential equations of motion into a single equation. Unfortunately, the fully coupled differential equations of motion of ACLD beams derived in Lee and Kim (1999) cannot be reduced into a single equation.

Thus, as the extension of the authors' previous work (Lee and Kim, 1999), this paper introduces a modal analysis method for the uniform ACLD beams. The appealing features of the present work include the followings. (1) Exact natural modes are spectrally formulated directly from the fully coupled equations of motion. (2) The orthogonality property of the spectrally formulated exact natural modes is derived to complete the present MAM. (3) The present MAM is verified by comparing with both FEM and SEM solutions of illustrative examples.

2. Coupled Dynamic Equations of Motion

Consider an ACLD beam element of length L, as shown in Fig. 1. The beam element consists of a VEM layer that is sandwiched between a PZT constraining layer and the base beam structure. In Fig. 1, h_b, h_v and h_p present the thicknesses of the base beam, the VEM layer, and the PZT layer, respectively. w is the flexural deflection of the base beam, and u_b, u_v and u_p are the axial displacements of the neutral axis of the base beam, the VEM layer, and the PZT layer, respectively. $\theta=\partial w/\partial x$ is the rotational angle of the base beam and Ψ is the shear angle of the VEM layer. The subscripts b, v and p will be continuously used in the following to represent the quantities for the base beam, VEM layer, and PZT layer, respectively.

A set of axial-bending-shear coupled dynamic equations of motion for the three-layer beam has been derived in the previous work by Lee and Kim (1999)

Equations of Motion

$$EI_w w''''+\rho A\ddot{w}+\alpha\ddot{u}_b'-\beta u'''-\gamma\ddot{w}''+\varepsilon_1\ddot{\psi}'-\varepsilon_2\phi'''=p(x,\ t)$$

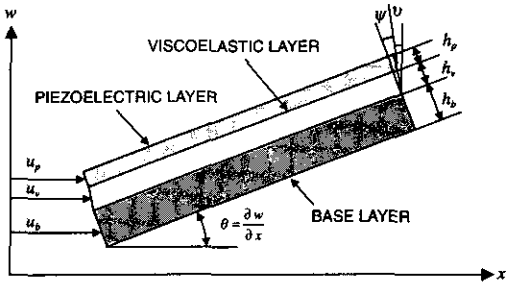

Fig. 1 The geometry and deformations of an ACLD beam

$$EAu_b''-\rho A\ddot{u}_b+\alpha\ddot{w}'-\beta w'''-\varepsilon_3\ddot{\psi}+\varepsilon_4\psi''=\tau(x,\ t) \tag{1}$$

$$EI_\psi\psi''-\rho I\ddot{\psi}+\varepsilon_1\ddot{w}'-\varepsilon_2 w'''-\varepsilon_3\ddot{u}_b+\varepsilon_4 u''-A_v(G\circ\psi)=r(x,\ t)$$

Boundary Conditions

$$N=\bar{N} \text{ or } u_b=\bar{u}_b,\ M=\bar{M} \text{ or } \theta=\bar{\theta} \tag{2}$$
$$R=\bar{R} \text{ or } \psi=\bar{\psi},\ Q=\bar{Q} \text{ or } w=\bar{w}$$

where prime (′) and dot (˙) indicate the partial derivatives with respect to the spatial coordinate x and time t, respectively. $p(x,\ t)$, $\tau(x,\ t)$ and $r(x,\ t)$ represent the transverse force, axial force, and the moment, respectively, all externally applied along the beam. The material and geometric properties used in Eq. (1) are defined as follows:

$$\begin{aligned}
&\rho A=\rho_b A_b+\rho_v A_v+\rho_p A_p,\\
&\rho I=\rho_v I_v+\rho_v A_v h_v^2/4+\rho_p A_p h_v^2\\
&\alpha=\rho_v A_v h_1/2+\rho_p A_p h_2/2,\\
&\beta=E_p A_v h_1/2+E_p A_p h_2/2\\
&\gamma=\rho_v I_v+\rho_v A_v h_1^2/4+\rho_p A_p h_2^2/4\\
&EI_w=E_b I_b+E_v I_v+C_{11}^D I_p+E_p A_p h_2{}^2/4,\\
&EI_\psi=E_v I_v+E_v A_v h_v^2/4+E_p A_p h_v^2\\
&EA=E_b A_b+E_v A_v+E_p A_p,\\
&E_p=C_{11}^D-h_{31}^2/\beta_{33}^S\\
&\varepsilon_1=\rho_v I_v+\rho_v A_v h_v h_1/4+\rho_p A_p h_v h_2/2,\\
&\varepsilon_2=E_v I_v+E_v A_v h_v h_1/4+E_p A_p h_v h_2/2\\
&\varepsilon_3=\rho_v A_v h_v/2+\rho_p A_p h_v,\\
&\varepsilon_4=E_v A_v h_v/2+E_p A_p h_v\\
&h_1=h_b+h_v,\ h_2=h_b+2h_v+h_p
\end{aligned} \tag{3}$$

where E, I, A, b, h and ρ(for each layer) are the Young's modulus, area moment of inertia about the neutral axis, cross-sectional area, width, thickness, and the mass density, respectively. C_{11}^D, β_{33}^S, and h_{31} are the elastic stiffness, the dielectric constant, and the piezoelectric constant, respectively.

In Eq. (2), N, Q, and M represent the axial force, transverse shear force, and the bending moment in the base beam, respectively, and R represents the bending moment in the VEM layer. They are related to the displacement fields as

$$\begin{aligned}
&N=EAu_b'-\beta w''+\varepsilon_4\psi'\\
&M=EI_w w''-\beta u_b'-\varepsilon_2\psi'\\
&Q=-M'+\gamma\ddot{w}'-\varepsilon_1\ddot{\psi}+\varepsilon_2\psi''\\
&R=EI_\psi\psi'-\varepsilon_2 w''+\varepsilon_4 u_b'
\end{aligned} \tag{4}$$

Similarly, $\bar{N}$, $\bar{Q}$, $\bar{M}$, and $\bar{R}$ in Eq. (2) represent the boundary forces and moments which are externally applied or piezoelectricity generated by the driving voltage supplied to PZT layer.

The last term of Eq. (1) represents the viscoelastic shear stress defined as (Christensen, 1982)

$$G\circ\psi=\int_{-\infty}^{t}G(t-\tau)\frac{\partial\psi(x,\ \tau)}{\partial\tau}d\tau \tag{5}$$

where $G(t)$ is the relaxation function of VEM, *i.e.*, the stress response to a unit-step strain input. In frequency domain, Eq. (5) can be expressed as follows:

$$G^*(i\omega)\Psi(x;\ \omega) \tag{6}$$

where $G^*(i\omega)$ is the complex modulus and Ψ is the spectral component of Ψ defined in Eq. (8).

3. Spectrally Formulated Exact Natural Modes

The natural modes and natural frequencies of a structure can be formulated from its eigenvalue problem. To formulate the eigenvalue problem, consider the free vibration of an ACLD beam.

$$EI_w w''''+\rho A\ddot{w}+\alpha\ddot{u}_b-\beta u'''-\gamma\ddot{w}''+\varepsilon_1\ddot{\psi}'-\varepsilon_2\psi'''=0$$

$$EAu_b''-\rho A\ddot{u}_b+\alpha\ddot{w}'-\beta w'''-\varepsilon_3\ddot{\psi}+\varepsilon_4\psi''=0 \tag{7}$$

$$EI_\psi\psi''-\rho I\ddot{\psi}+\varepsilon_1\ddot{w}'-\varepsilon_2 w'''-\varepsilon_3\ddot{u}_b+\varepsilon_4 u''-A_v(G\circ\psi)=0$$

The general solutions of Eq. (7) can be assumed in the spectral representations as

$$\begin{aligned}
&w(x,\ t)=\sum_{s=1}^{S}W_s(x)e^{i\omega st}\\
&u_b(x,\ t)=\sum_{s=1}^{S}U_s(x)e^{i\omega st}\\
&\psi(x,\ t)=\sum_{s=1}^{S}\Psi_s(x)e^{i\omega st}
\end{aligned} \tag{8}$$

where W_s, U_s and Ψ_s are the spectral components of w, u_b, and ψ, respectively, all corresponding to the discrete frequency $\omega_s=2\pi s/T$. S is the total number of spectral components to be taken into account in the spectral analysis. The time window T is related to S by

$$S=2f_{\text{NYQ}}T \tag{9}$$

where f_{NYQ} is the Nyquest frequency in Hz. The accuracy of time responses depends on how many

spectral components are taken into account in the analysis. For shorthand, the subscript s, which indicates the spectral components of a quantity, will be omitted in the following.

Substituting Eq. (8) into Eq. (7) and removing the common time-dependent factors gives three coupled ordinary differential equations:

$$\begin{aligned} &EI_w W'''' - \omega^2 \rho A W = \omega^2(\alpha U' - \gamma W'' \\ &\quad + \varepsilon_1 \Psi') + \beta U''' + \varepsilon_2 \Psi''' \\ &EAU'' + \omega^2 \rho A U = \omega^2(\alpha W' - \varepsilon_3 \Psi) \\ &\quad + \beta W''' - \varepsilon_4 \Psi'' \\ &EI_\phi \Psi'' + \omega^2 \rho I \Psi = \omega^2(\varepsilon_1 W' - \varepsilon_3 U'') \\ &\quad + \varepsilon_2 W''' - \varepsilon_4 U'' + A_v G^* \Psi \end{aligned} \tag{10}$$

Let the general solutions of above equations be

$$\begin{aligned} W(x) &= \sum_{i=1}^{8} A_i e^{k_i x} \\ U(x) &= \sum_{i=1}^{8} B_i e^{k_i x} \\ \Psi(x) &= \sum_{i=1}^{8} C_i e^{k_i x} \end{aligned} \tag{11}$$

where $k_i (i = 1, 2, \cdots, 8)$ are the wave numbers and they are determined from the dispersion relation:

$$a_1 k^8 + a_2 k^6 + a_3 k^4 + a_4 k^2 + a_5 = 0 \tag{12}$$

where

$$\begin{aligned} a_1 &= EI_u EI_w EI_\phi - \varepsilon_4^2 EI_w + 2\beta\varepsilon_2\varepsilon_4 - EA\varepsilon_2^2 - EI_\phi \beta^2 \\ a_2 &= \omega^2(-\rho I \beta^2 + 2\beta\varepsilon_1\varepsilon_4 - \gamma\varepsilon_4^2 + \rho I EAEI_w \\ &\quad - 2EI_w\varepsilon_3\varepsilon_4 - 2EA\varepsilon_1\varepsilon_2 + 2\beta\varepsilon_2\varepsilon_3 + 2\alpha\varepsilon_2\varepsilon_4 \\ &\quad - \rho A\varepsilon_2^2 + \varepsilon EAEI_\phi - 2\alpha\beta EI_\phi + \rho AEI_w EI_\phi) \\ &\quad + i\omega A_v G^*(\omega)(EAEI_w - \beta^2) \\ a_3 &= \omega^4(\rho IEI_u\gamma - \varepsilon_1^2 EA + 2\beta\varepsilon_3\varepsilon_1 - 2\rho I\alpha\beta - 2\gamma\varepsilon_1\varepsilon_4 \\ &\quad + 2\alpha\varepsilon_1\varepsilon_4 - \varepsilon_3^2 EA + \rho A\rho IEI_w + 2\alpha\varepsilon_2\varepsilon_3 \\ &\quad - 2\rho A\varepsilon_1\varepsilon_2 - \alpha^2 EI_\phi + \rho AEI_\phi\gamma) + i\omega^3 A_v G^*(\omega) \\ &\quad (\gamma EA - 2\alpha\beta + \rho AEI_w) + w^2(\rho A\varepsilon_4^2 \\ &\quad - \rho AEAEI_\phi) \\ a_4 &= \omega^6(2\alpha\varepsilon_1\varepsilon_3 - \varepsilon_3^2\gamma - \rho A\varepsilon_1^2 + \alpha^2\rho I + \gamma\rho A\rho I) \\ &\quad + \omega^4(2\rho A\varepsilon_3\varepsilon_4 - \rho A\rho IEA - \rho I^2 EI_\phi) \\ &\quad + i\omega^5 A_v G^*(\omega)(\rho A\gamma - \alpha^2) - i\omega^3 \rho AEAA_v G^*(\omega) \\ a_5 &= \omega^6(\rho A\varepsilon_3^2 - \rho A^2\rho I) - i\omega^5 \rho A^2 A_v G^*(\omega) \end{aligned} \tag{13}$$

Eq. (12) gives eight values of k at a specified frequency ω, but they always appear as $\pm$ pairs. Thus, the general solutions of Eq. (9) can be rewritten as

$$W(x) = \sum_{i=1}^{4}(A_i e^{k_i x} + A_{2i} e^{-k_i x}) = [\Phi(x)]\{A\}$$

$$U(x) = \sum_{i=1}^{4}(B_i e^{k_i x} + B_{2i} e^{-k_i x}) = [\Phi(x)]\{B\} \tag{14}$$

$$\Psi(x) = \sum_{i=1}^{4}(C_i e^{k_i x} + C_{2i} e^{-k_i x}) = [\Phi(x)]\{C\}$$

where

$$\begin{aligned} [\Phi(x)] &= [e^{k_1 x}\ e^{-k_1 x}\ e^{k_2 x}\ e^{-k_2 x}\ e^{k_3 x} \\ &\qquad e^{-k_3 x}\ e^{k_4 x}\ e^{-k_4 x}] \\ \{A\} &= \{A_1\ A_2\ A_3\ A_4\ A_5\ A_6\ A_7\ A_8\}^T \\ \{B\} &= \{B_1\ B_2\ B_3\ B_4\ B_5\ B_6\ B_7\ B_8\}^T \\ \{C\} &= \{C_1\ C_2\ C_3\ C_4\ C_5\ C_6\ C_7\ C_8\}^T \end{aligned} \tag{15}$$

The complex modulus G^* can be represented by using an appropriate VEM model such as the GHM representation (McTavish and Hughes, 1993):

$$G^* = \varkappa\left[1 + \sum_{r=1}^{n} \alpha_r \frac{s^2 + 2\hat{\xi}_r\hat{\omega}_r s}{s^2 + 2\hat{\xi}_r\hat{\omega}_r s + \hat{\omega}_r^2}\right] \tag{16}$$

where $s = i\omega$ is the Laplace variable and the parameters $\varkappa$, α_r, $\hat{\xi}_r$, and $\hat{\omega}_r$ are determined to match the experimentally measured damping data accurately. The accuracy of GHM model should depend on how many dissipation variables (*i.e.*, the value of n) are used in the model. In this paper, the GHM model with a single dissipation variable (*i.e.*, $n = 1$) will be considered for numerical illustrations.

The relations between the coefficients $\{A\}$, $\{B\}$, and $\{C\}$ can be derived, by substituting Eq. (14) into Eq. (10), as

$$\begin{aligned} \{B\} &= [diagonal(\lambda_i)]\{A\} \\ \{C\} &= [diagonal(\mu_i)]\{A\} \end{aligned} \tag{17}$$

where

$$\begin{aligned} \lambda_i &= (-1)^i[(\beta\varepsilon_2 - EI_w\varepsilon_4)k_i^6 + \omega^2(\beta\varepsilon_1 - \alpha\varepsilon_2 \\ &\quad - EI_w\varepsilon_3 - \gamma\varepsilon_4)k_i^4 + \{(\alpha\varepsilon_1 - \gamma\varepsilon_3)\omega^4 \\ &\quad + \rho A\varepsilon_4\omega^2\}k_i^2 + \rho A\varepsilon_3\omega^4]/\Delta_i \\ \mu_i &= (-1)^i[(EAEI_w - \beta^2)k_i^6 + \omega^2(EA\gamma \\ &\quad + \rho AEI_w - 2\alpha\beta)k_i^4 - \{(\alpha^2 - \gamma\rho A)\omega^4 \\ &\quad + \rho AEA\omega^2\}k_i^2 - \rho A^2\omega^4]/\Delta_i \\ \Delta_i &= \{(EA\varepsilon_2 - \beta\varepsilon_4)k_i^4 + \omega^2(EA\varepsilon_1 + \rho A\varepsilon_2 - \beta\varepsilon_3 \\ &\quad - \alpha\varepsilon_4)k_i^2 + \omega^4(\rho A\varepsilon_1 - \alpha\varepsilon_3)\}k_i \end{aligned} \tag{18}$$

The functions $\lambda_i(x)$ and $\mu_i(x)$ indicate the degree of coupling between three displacement fields. Infinite or zero values of $\lambda_i(x)$ and $\mu_i(x)$ simply imply de-coupling.

By substituting Eq. (17) into Eq. (14), the general solutions can be expressed all in terms of

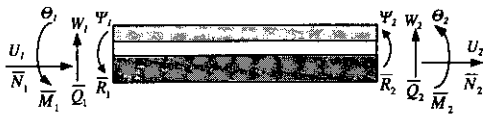

Fig. 2 Spectral element of ACLD beam

coefficients $\{A\}$ as follows:

$$\begin{aligned} W(x)&=[\Phi(x)]\{A\} \\ U(x)&=[\Phi(x)][diagonal(\lambda_i^{-1})]\{A\} \\ \Psi(x)&=[\Phi(x)][diagonal(\mu_i^{-1})]\{A\} \end{aligned} \quad (19)$$

The coefficients $\{A\}$ can be determined from boundary conditions. By using Eq. (19), the spectral nodal DOFs (degrees of freedom) defined in Fig. 2 can be expressed in terms of $\{A\}$ as

$$\{y\}=[P(\omega)]\{A\} \quad (20)$$

where

$$\{y\}=\{U_1\ W_1\ \Theta_1\ \Psi_1\ U_2\ W_2\ \Theta_2\ \Psi_2\}^T \quad (21)$$

The matrix $[P]$ is frequency-dependent and is given in Appendix. The coefficients $\{A\}$ can be eliminated from Eq. (19) by using Eq. (20). This gives the general solutions in terms of the spectral nodal DOFs as

$$\begin{aligned} W(x)&=[\Phi(x)][P(\omega)]^{-1}\{y\}=[N_w(x;\ \omega)]\{y\} \\ U(x)&=[\Phi(x)][diagonal(\lambda_i^{-1})][P(\omega)]^{-1}\{y\} \\ &=[N_u(x;\ \omega)]\{y\} \\ \Psi(x)&=[\Phi(x)][diagonal(\lambda_i^{-1})][P(\omega)]^{-1}\{y\} \\ &=[N_\psi(x;\ \omega)]\{y\} \end{aligned} \quad (22)$$

where $[N_w]$, $[N_u]$, and $[N_\psi]$ are the frequency-dependent (dynamic) shape functions matrices. They are considered to be *exact* because they are so formulated that Eq. (22) satisfies both the governing equations and the boundary conditions at nodes exactly.

Substituting Eq. (22) into the force-displacement relations of Eq. (4), the spectral nodal forces and moments defined in Fig. 2 can be written in terms of $\{A\}$ as

$$\{f\}=[Q(\omega)]\{A\} \quad (23)$$

where

$$\{f\}=\{\bar{N}_1\ \bar{Q}_1\ \bar{M}_1\ \bar{R}_1\ \bar{N}_2\ \bar{Q}_2\ \bar{M}_2\ \bar{R}_2\}^T \quad (24)$$

In Eq. (24), $\bar{N}_i$, $\bar{Q}_i$, $\bar{M}_i$ and $\bar{R}_i (i=1, 2)$ are the spectral nodal forces and moments defined in Fig. 2. The frequency-dependent matrix $[Q]$ is tabulated in Appendix.

From Eqs. (20) and (23), the spectral nodal force-displacement relation can be obtained as

$$\{f\}=[Q(\omega)][P(\omega)]^{-1}\{y\}=[K(\omega)]\{y\} \quad (25)$$

where $[K]=[Q][P]^{-1}$ is the dynamic stiffness matrix computed at each discrete frequency and, in SEM, it is often called *spectral element matrix*. Computer implementation to obtain the spectral element matrix can be readily accomplished either numerically or algebraically. To formulate the spectral element matrix in an explicit form is often tedious, but now it has become easy thanks to the recent advances in symbolic computing (Wolfram, 1996). Since the explicit expression of $[K]$ is too lengthy, it will not be listed herein. Applying boundary conditions into Eq. (25) gives the system equation in the reduced form as

$$\{\bar{f}\}=[\bar{K}(\omega)]\{\bar{y}\} \quad (26)$$

The eigensolutions (*i.e.*, natural frequencies and natural modes) are required to conduct the modal analysis. To form an eigenvalue problem, enforce all nodal forces to be zero. This may yield an eigenvalue problem in the form

$$[\bar{K}(\omega)]\{\bar{y}\}=\{0\} \quad (27)$$

The natural frequencies, $\omega_n (n=1, 2, \cdots, \infty)$, can be obtained numerically from the roots of the determinant of $[\bar{K}]$. At each natural frequency, eight wave-numbers $\pm k_i (i=1, 2, 3, 4)$ are obtained from the dispersion relation of Eq. (12). The eigenvector $\{\bar{y}\}$ corresponding to a natural frequency can be computed by substituting the natural frequency into Eq. (27). Applying the eigenvectors $\{\bar{y}\}$ and corresponding wave-numbers k_i, all computed at each natural frequency, into Eq. (22) gives the natural modes. The natural modes are considered *exact* in the sense that no approximations have been considered in the formulation procedure. One reminds that the natural modes computed from Eq. (22) are the 'damped natural modes' into which the effects of viscoelastic layer damping are already smeared in the process of spectral formulation.

4. Orthogonality of Natural Modes

In the preceding section, the exact (damped) natural modes are spectrally formulated. To complete the modal analysis method for fully coupled structural dynamics problems, the orthogonality property of natural modes is derived in the following.

Since the eigensolution should satisfy its eigenvalue problem, Eq. (10) can be written for the n-th eigensolution as follows:

$$\begin{aligned}
&\omega_n^2(\rho A W_n+\alpha U_n'-\gamma W_n''+\varepsilon_1\Psi_n')=M_n''\\
&\omega_n^2(\rho A U_n-\alpha W_n'+\varepsilon_3\Psi_n)=-N_n'\\
&\omega_n^2(\rho I\Psi_n+\varepsilon_3 U_n'-\varepsilon_1 W_n')=-R_n'+A_v G^*\Psi_n
\end{aligned}\tag{28}$$

where N_n, Q_n, M_n and R_n are the internal forces and moments computed from Eq. (4) at the n-th natural frequency. On multiplying Eq. (30) by W_m, U_m, and Ψ_m in order, integrating the results from $x=0$ to L, applying the integral by parts yields, and summing up final forms of three equations yields

$$\begin{aligned}
&\omega_n^2\int_0^L\{\rho A U_n U_m+\rho A W_n W_m+\rho I\Psi_n\Psi_m\\
&\quad-\alpha(U_n W_m'+U_n W_m')-\varepsilon_1(W_m'\Psi_n+W_n'\Psi_m)\\
&\quad+\varepsilon_3(U_n\Psi_m+U_n\Psi_m)+\gamma W_n' W_m'\}dx\\
&\quad=-N_n U_m|_0^L-Q_n W_m|_0^L-M_n W_m'|_0^L-R_n\Psi_m|_0^L\\
&\quad+\int_0^L M_n W_m''dx+\int_0^L N_n U_m'dx+\int_0^L R_n\Psi_m'dx\\
&\quad+A_v G^*\int_0^L\Psi_n\Psi_m dx
\end{aligned}\tag{29}$$

For the m-th eigensolution, a similar procedure may yield an equation that can be readily reduced from Eq. (29) by replacing (m, n) with (n, m). Subtract the equation for the n-th eigensolution from that for the m-th eigensolution and then apply the boundary conditions to obtain the orthogonality property as follows:

$$\begin{aligned}
&\int_0^L\{\rho A(U_n U_m+W_n W_m)+\rho I\Psi_n\Psi_m-\alpha(U_n W_m'\\
&\quad+U_m W_n')-\varepsilon_1(W_n'\Psi_m+W_m'\Psi_n)+\varepsilon_3(U_n\Psi_m\\
&\quad+U_m\Psi_m)+\gamma W_n' W_m'\}dx=m_n\delta_{nm}
\end{aligned}\tag{30}$$

where δ_{mn} is the Kronecker delta and m_n is the n-th modal mass defined by

$$\begin{aligned}
m_n=\int_0^L\{&\rho A(U_n^2+W_n^2)+\rho I\Psi_n^2-2\alpha U_n W_n'\\
&-2\varepsilon_1 W_n'\Psi_n+2\varepsilon_3 U_n\Psi_n+\gamma W_n'^2\}dx
\end{aligned}\tag{31}$$

5. Modal Equations

The forced vibration of an ACLD beam is represented by Eq. (1). By using the orthogonality property of the spectrally formulated exact (damped) natural modes, the modal equations for the ACLD beam will be derived in this section.

By superposing the natural modes, the forced vibration responses can be assumed in the forms

$$\begin{aligned}
w(x,\ t)&=\sum_{n=1}^{\infty}W_n(x)q_n(t)\\
u_b(x,\ t)&=\sum_{n=1}^{\infty}U_n(x)q_n(t)\\
\phi(x,\ t)&=\sum_{n=1}^{\infty}\Psi_n(x)q_n(t)
\end{aligned}\tag{32}$$

where W_n, U_n, and Ψ_n are the n-th natural modes. $q_n(t)$ are the modal coordinates and they can be expressed in the spectral representation:

$$q_n(t)=\sum_{s=1}^{N}\tilde{q}_{ns}e^{i\omega_s t}\tag{33}$$

where $\tilde{q}_{ns}$ are the spectral components of n-th modal coordinate. Substituting Eq. (33) into Eq. (32) gives

$$\begin{aligned}
w(x,\ t)&=\sum_{n=1}^{\infty}\sum_{s=1}^{N}W_n(x)\,\tilde{q}_{ns}e^{i\omega_s t}\\
u_b(x,\ t)&=\sum_{n=1}^{\infty}\sum_{s=1}^{N}U_n(x)\,\tilde{q}_{ns}e^{i\omega_s t}\\
\phi(x,\ t)&=\sum_{n=1}^{\infty}\sum_{s=1}^{N}\Psi_n(x)\,\tilde{q}_{ns}e^{i\omega_s t}
\end{aligned}\tag{34}$$

Similarly, the external forces can be expressed in the spectral representations as

$$\begin{aligned}
p(x,\ t)&=\sum_{s=1}^{N}\tilde{p}_s(x)e^{i\omega_s t}\\
\tau(x,\ t)&=\sum_{s=1}^{N}\tilde{\tau}_s(x)e^{i\omega_s t}\\
r(x,\ t)&=\sum_{s=1}^{N}\tilde{r}_s(x)e^{i\omega_s t}
\end{aligned}\tag{35}$$

where $\tilde{p}_s$, $\tilde{\tau}_s$, and $\tilde{r}_s$ are the spectral components.

Substituting Eqs. (34) and (35) into Eq. (1) and applying Eq. (4) yields the equations, for the s-th spectral component, as

$$\begin{aligned}
&\sum_{n=1}^{\infty}M_n''\,\tilde{q}_{ns}-\omega_s^2\sum_{n=1}^{\infty}(\rho A W_n+\alpha U_n'-\gamma W_n''\\
&\quad+\varepsilon_1\Psi_n')\,\tilde{q}_{ns}=\tilde{p}_s(x)
\end{aligned}$$

$$\sum_{n=1}^{\infty} N_n' \tilde{q}_{ns} + \omega_s^2 \sum_{n=1}^{\infty} (\rho A U_n - \alpha W_n' + \varepsilon_3 \Psi_n) \tilde{q}_{ns} = \tilde{\tau}_s(x) \tag{36}$$

$$\sum_{n=1}^{\infty} (R_n' - A_v G^* \Psi_n) \tilde{q}_{ns} + \omega_s^2 \sum_{n=1}^{\infty} (\rho I \Psi_n - \varepsilon_1 W_n' + \varepsilon_3 U_n) \tilde{q}_{ns} = \tilde{r}_s(x)$$

On multiplying Eq. (36) by the m-th natural modes, W_m, U_m, and Ψ_m in order, integrating the results from $x=0$ to L, and taking a lengthy manipulation may yield

$$-\sum_{n=1}^{\infty} (\omega_s^2 - \omega_n^2) \tilde{q}_{ns} \int_0^L (\rho A W_n W_m - \alpha U_n W_m' + \gamma W_n' W_m' - \varepsilon_1 W_n' \Psi_m) dx = \int_0^L \tilde{p}_s(x) W_m dx$$

$$\sum_{n=1}^{\infty} (\omega_s^2 - \omega_n^2) \tilde{q}_{ns} \int_0^L (\rho A U_n U_m - \alpha U_m W_n' + \varepsilon_3 U_m \Psi_n) dx = \int_0^L \tilde{\tau}_s(x) U_m dx \tag{37}$$

$$\sum_{n=1}^{\infty} (\omega_s^2 - \omega_n^2) \tilde{q}_{ns} \int_0^L (\rho I \Psi_n \Psi_m - \varepsilon_1 W_n' \Psi_m + \varepsilon_3 U_n \Psi_m) dx = \int_0^L \tilde{r}_s(x) \Psi_m dx$$

Subtract the last two equations of (37) from the first equation and apply the orthogonality property of Eq. (30) into Eq. (39) to obtain

$$\tilde{q}_{ns} = \frac{\tilde{f}_{ns}}{m_n(\omega_n^2 - \omega_s^2)} \quad (s=1, 2, \cdots, N \text{ and } n=1, 2, \cdots, \infty) \tag{38}$$

where

$$\tilde{f}_{ns} = \int_0^L \{\tilde{p}_s(x) W_n - \tilde{\tau}_s(x) U_n - \tilde{r}_s(x) \Psi_n\} dx \tag{39}$$

Substituting spectral components $\tilde{q}_{ns}$ into Eq. (33) gives the modal coordinates in the time domain. This computation can be accomplished efficiently by use of IFFT algorithm.

By using Eqs. (33) and (35), Eq. (38) can be transformed into the modal equations in the time domain as

$$\ddot{q}_n(t) + \omega_n^2 q_n(t) = \frac{f_n(t)}{m_n} \tag{40}$$

where ω_n is the n-th natural frequency and $f_n(t)$ is the corresponding modal force defined by

$$f_n(t) = \int_0^L \{p(x, t) W_n - \tau(x, t) U_n - r(x, t) \Psi_n\} dx \tag{41}$$

One reminds that, because the effects of viscoelastic layer damping are already smeared into the (damped) natural modes, Eq. (41) does not contain the first-order derivative term.

6. Numerical Illustrations

In this paper, a cantilevered uniform ACLD (three-layer) beam is considered for numerical illustrations. The base beam is fully covered with VEM layer from the fixed root to the free end, and the VEM layer is also fully covered fully with PZT layer. The VEM layer is represented by one -term GHM model. The ACLD beam has the length of $L=261.6$ *mm*. The base beam, VEM layer, and PZT layer all have the same width of 12.7 *mm*. The geometry and material properties of the base beam are : thickness $h_b=2.86$ *mm*, Young's modulus $E_b=71$ *GPa*, and mass density $\rho_b=2700$ *kg/m*^{3}. The PZT layer has the thickness $h_p=0.762$ *mm*, Young's modulus $E_p=64.9$ *GPa*, elastic stiffness $C_{11}^p=74$ *GPa*, piezoelectric constant $d_{31}=-175\times10^{-12}$ *m/V*, and mass density $\rho_p=7600$ *kg/m*^{3}. The VEM layer is made of 3M ISD 112, and it has the thickness $h_v=0.25$ *mm*, and mass density $\rho_v=1250$ *kg/m*^{3}.

First, to confirm the accuracy of the present spectral element formulation, Table 1 and Fig. 3 compare the frequency response functions (FRF) and natural frequencies of the ACLD beam obtained by SEM and FEM, respectively. For SEM, the FRF are obtained from Eq. (26) and

Table 1 Comparison of the natural frequencies of a cantilevered uniform ACLD beam obtained by using spectral element method (SEM) and conventional finite element method (FEM) (n=total number of finite elements used in the analysis)

Mode	ω_{FEM}(Hz)			ω_{SEM} (Hz)
	$n=10$	$n=20$	$n=50$	
1 st	28.3	28.3	28.3	28.3
2 nd	162.2	161.4	161.2	161.2
3 rd	429.5	425.0	423.8	423.5
4 th	803.2	785.8	781.1	780.2
5 th	1306.8	1256.6	1243.3	1240.8

the natural frequencies from Eq. (27). Since the ACLD beam is uniform, a single spectral element is enough to get exact solutions, which has been well proved in previous works (Doyle, 1997; Banerjee *et al.*, 1996). To obtain the FRF in Fig. 3, the ACLD beam is excited by applying a point load on its free end. Figure 3 shows that, as we increase the total number of finite elements used in FEM, the finite element solutions indeed converge to the FRF obtained by SEM. Similarly, Table 1 shows that the natural frequencies obtained by FEM also converge to those obtained by SEM as the total number of finite elements in FEM is increased. These observations may prove the accuracy and validity of the present spectral element formulation. Thus, the solutions obtained by SEM can be considered *exact* and they will be used as the reference to evaluate the accuracy and validity of the present MAM.

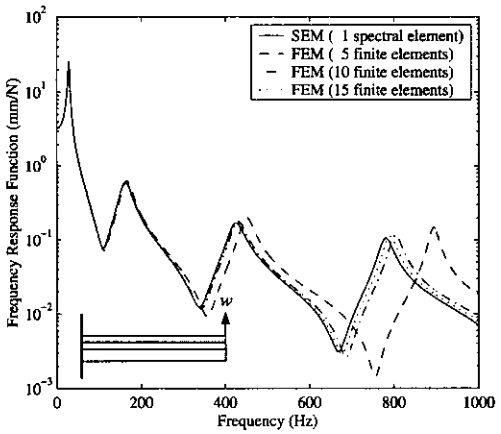

Fig. 3 Comparison of the frequency response functions of an ACLD beam obtained by spectral element method (SEM) and conventional finite element method (FEM)

Tables 2 and 3 show the natural frequencies and modal dampings of the ACLD beam computed from Eq. (27) with varying the thickness of VEM layer. As the thickness of VEM layer is gradually decreased to zero, in general, the natural frequencies of the ACLD beam are found to be gradually increased and they converge to the values for the two-layer active beam considered by Lee and Kim (2000b). Table 3 also shows, as expected, that the modal damping converges to zero values as the VEM thickness is reduced to zero.

Figure 4 shows the solution accuracy of the present MAM, depending on how many normal modes are used in the analysis. The FRF obtained by MAM are compared with accurate SEM solutions. The FRF by MAM are given by $\sum_{n}^{N} W_n(x=L)\,\tilde{q}_{ns}/\tilde{p}_s(x=L)$ from Eqs. (34) and (35), where N is the number of normal modes used in MAM. As expected, the FRF obtained by MAM converge to the exact one as we increase

Table 3 Viscoelastic-layer thickness dependence of modal damping for a cantilevered uniform ACLD beam

Mode	$\xi_{Three-Layer}$		
	h_v=0.25 *mm*	h_v=0.025 *mm*	h_v=0.0025 *mm*
1 st	0.0559	0.0114	0.0014
2 nd	0.0776	0.1321	0.0431
3 rd	0.0395	0.0171	0.0025
4 th	0.0191	0.0131	0.0022
5 th	0.0095	0.0099	0.0021

Table 2 Viscoelastic-layer thickness dependence of natural frequency for a cantilevered uniform ACLD beam

Mode	$\omega_{Three-Layer}$(Hz)			$\omega_{Two-Layer}$(Hz) (Lee & Kim, 2000b)
	h_v=0.25 *mm*	h_v=0.025 *mm*	h_v=0.0025 *mm*	
1 st	28.34	29.75	30.01	30.04
2 nd	161.16	166.41	171.75	188.22
3 rd	423.52	497.69	523.14	526.89
4 th	780.23	938.50	1018.45	1031.13
5 th	1240.79	1492.23	1669.98	1705.41

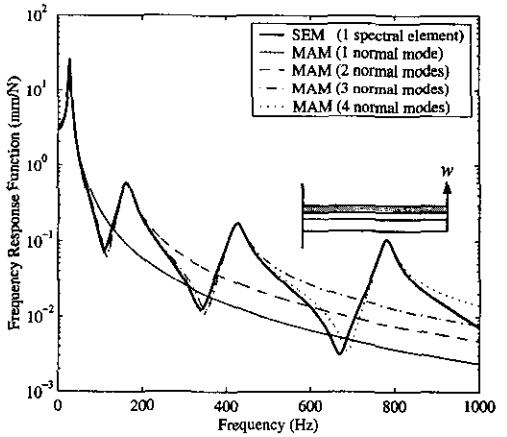

Fig. 4 Comparison of the frequency response functions of an ACLD beam obtained by spectral element method (SEM) and modal analysis method (MAM)

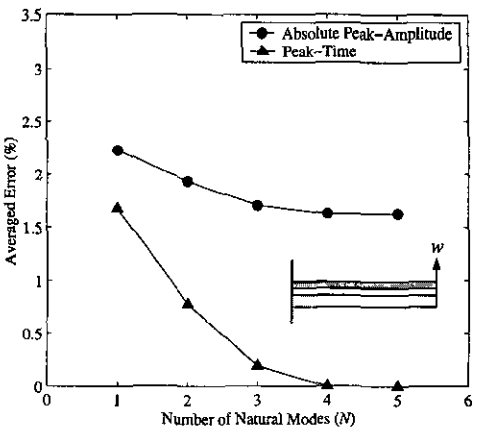

Fig. 5 Accuracy of the dynamic responses of an ACLD beam obtained by modal analysis method (MAM), when compared with the result obtained by spectral element method (SEM)

the total number of exact natural modes considered in MAM. Figure 5 shows the accuracy of the dynamic responses predicted by MAM, depending on the total number of exact natural modes considered in MAM. The dynamic response in the time domain can be characterized by its peak-amplitudes and peak-times at which the peak-amplitudes occur. Thus, to evaluate the accuracy of the dynamic responses obtained by MAM (with respect to the exact solution by SEM), two errors are defined herein. The first one is the averaged absolute peak-amplitude error, which is obtained by averaging the differences of the absolute peak-amplitudes obtained by MAM and SEM. The second one is the averaged peak-time error, which is obtained by averaging the differences of the peak-times obtained by MAM and SEM. To compute the time-averaged errors shown in Fig. 5, the first fifteen peaks of dynamic response are considered. As we include more exact natural modes for the modal analysis, Fig. 5 shows that both averaged errors become smaller.

Equation (40) shows that the accuracy of the vibration amplitude strongly depends on the accuracy of the modal mass computed from Eq. (31). However, the computation error is inevitable due to the numerical integration required to compute the modal mass. This is the main reason why the averaged absolute peak-amplitude error still keeps its value about 1.7% though we consider more than four exact natural modes in the modal analysis, while the averaged peak-time error almost disappears. Thus, improving the accuracy of the modal mass may further improve the solution accuracy of the present MAM, which is based on spectrally formulated exact natural modes.

7. Conclusions

This paper introduces a modal analysis method for ACLD beams. The exact natural modes are spectrally formulated by using the exact wave solutions of a set of fully coupled equations of motion. To complete the modal analysis method, the orthogonality of the spectrally formulated exact natural modes is derived. By using the orthogonality of natural modes, the modal equations for the forced vibration are derived. A cantilevered uniform ACLD beam is considered as an example problem to evaluate the modal analysis method introduced in this paper. First it is observed that the finite element solutions indeed converge to the SEM solutions as the number of finite elements used in FEM is increased, which may prove the accuracy of SEM. The accuracy of the present MAM is then evaluated by comparing the MAM solutions with the

accurate SEM solutions. It is numerically shown that the present MAM provides very accurate solutions, which is thanks to the use of spectrally formulated exact natural modes and modal masses.

References

Banerjee, J. R., 1989, "Coupled Bending-Torsional Dynamic Stiffness Matrix for Beam Elements," *International Journal for Numerical Methods in Engineering*, Vol. 28, pp. 1283~1298.

Banerjee, J. R., Guo, S. and Howson, W. P., 1996, "Exact Dynamic Stiffness Matrix of a Bending-Torsion Coupled Beam Including Warping," *Computers & Structures*, Vol. 59, No. 4, pp. 613~621.

Banerjee, J. R., 1997, "Dynamic Stiffness Formulation for Structural Elements: A General Approach," *Computers & Structures*, Vol. 63, No. 1, pp. 101~103.

Baz, A., 1993, "Active Constrained Layer Damping," *Proc. Damping '93*, San Francisco, CA, pp. 187~209.

Bishop, R. E. D., Cannon, S. M., and Miao, S., 1989, "On Coupled Bending and Torsional Vibration of Uniform Beams," *Journal of Sound and Vibration*, Vol. 131, No. 3, pp. 457~464.

Christensen, R. M., 1982, *Theory of Viscoelasticity: an Introduction*, 2nd ed., Academic Press, Inc., New York.

Crawley, E. F. and de Luis, J., 1987, "Use of Piezoelectric Actuators as Elements of Intelligent Structures," *AIAA Journal*, Vol. 25, No. 10, pp. 1373~1385.

Dokumaci, E., 1987, "An Exact Solution for Coupled Bending and Torsion Vibrations of Uniform Beams Having Single Cross-Sectional Symmetry," *Journal of Sound and Vibration*, Vol. 119, No. 3, pp. 443~449.

Doyle, J. F., 1988, "A Spectrally Formulated Finite Element for Longitudinal Wave Propagation," *International Journal of Analytical and Experimental Modal Analysis*, Vol. 3, pp. 1~5.

Doyle, J. F., 1997, *Wave Propagation in Structures*, 2nd Ed., Springer-Verlag, New York.

Lee, U., 1998, "Equivalent Continuum Representation of Lattice Beams: Spectral Element Approach," *Engineering Structures*, Vol. 20, No. 7, pp. 587~592.

Lee, U., 2000, "Spectral Element Methods in Structural Dynamics," *The Shock and Vibration Digest* (in press).

Lee, U. and Kim, J., 2000a, "Determination of Non-Ideal Structural Boundary Conditions: a Spectral Element Approach," *AIAA Journal*, Vol. 38, No. 2, pp. 309~316.

Lee, U. and Kim, J., 2000b, "Dynamics of Elastic-Piezoelectric Two Layer Beams Using Spectral Element Method," *International Journal of Solids and Structures*, Vol. 37, pp. 4403~4417.

Lee, U. and Kim, J., 1999, "Spectral Element Modeling for the Beams Treated with Active Constraining Layer Damping," Proc. AIAA/ASME/AHS Adaptive Structures Forum, St. Louis, MO, AIAA-99-1541 (also in *International Journal of Solids and Structures*, in press).

Lee, U. and Lee, J., 1999, "Spectral-Element Method for Levy-Type Plates Subject to Dynamic Loads," *Journal of Engineering Mechanics*, Vol. 125, No. 2, pp. 243~247.

Lesieutre, G. A. and Lee, U., 1996, "A Finite Element for Beams Having Segmented Active Constrained Layers with Frequency-Dependent Viscoelastics," *Smart Structures and Materials*, Vol. 5, pp. 615~627.

Liao, W. H., 1997, "Active-Passive Hybrid Structural Control: An Enhanced Active Constrained Layer Damping Treatment with Edge Elements," *Ph. D. Thesis*, The Pennsylvania State University, PA.

McTavish, D. J. and Hughes, P. C., 1993, "Modeling of Linear Viscoelastic Space Structures," *Journal of Vibration and Acoustics*, Vol. 115, pp. 103~110.

Robbins, D. H. and Reddy, J. N., 1991, "Analysis of Piezoelectrically Actuated Beams Using a Layer-Wise Displacement Theory," *Computers & Structures*, 1991, Vol. No. 2, pp. 265~279.

Wolfram, S., 1996, *The Mathematica Book*, 3rd ed., Wolfram Media/Cambridge University

Press.

Appendix

The matrices $[\boldsymbol{P}]$ and $[\boldsymbol{Q}]$ in Eqs. (20) and (23) are defined as follows:

$$[\boldsymbol{P}]=\begin{bmatrix}
\lambda_1 & -\lambda_1 & \lambda_2 & -\lambda_2 & \lambda_3 \\
1 & 1 & 1 & 1 & 1 \\
k_1 & -k_1 & k_2 & -k_2 & k_3 \\
\mu_1 & -\mu_1 & \mu_2 & -\mu_2 & \mu_3 \\
e^{Lk_1}\lambda_1 & -e^{Lk_1}\lambda_1 & e^{Lk_2}\lambda_2 & -e^{-Lk_2}\lambda_2 & e^{Lk_3}\lambda_3 \\
e^{Lk_1} & e^{-Lk_1} & e^{Lk_2} & e^{-Lk_2} & e^{Lk_3} \\
e^{Lk_1}k_1 & -e^{-Lk_1}k_1 & e^{Lk_2}k_2 & -e^{-Lk_2}k_2 & e^{Lk_3}k_3 \\
e^{Lk_1}\mu_1 & -e^{-Lk_1}\mu_1 & e^{Lk_2}\mu_2 & -e^{-Lk_2}\mu_2 & e^{Lk_3}\mu_3
\end{bmatrix}$$

$$\begin{bmatrix}
-\lambda_3 & \lambda_4 & -\lambda_4 \\
1 & 1 & 1 \\
-k_3 & k_4 & -k_4 \\
-\mu_3 & \mu_4 & -\mu_4 \\
-e^{-Lk_3}\lambda_3 & e^{Lk_4}\lambda_4 & -e^{-Lk_4}\lambda_4 \\
e^{-Lk_3} & e^{Lk_4} & e^{-Lk_4} \\
-e^{Lk_3}k_3 & e^{Lk_4}k_4 & -e^{-Lk_4}k_4 \\
-e^{Lk_3}\mu_3 & e^{Lk_4}\mu_4 & -e^{-Lk_4}\mu_4
\end{bmatrix} \tag{A1}$$

$$[\boldsymbol{Q}]=\begin{bmatrix}
p_{11} & p_{11} & p_{12} & p_{12} \\
p_{21} & -p_{21} & p_{22} & -p_{22} \\
p_{31} & p_{31} & p_{32} & p_{32} \\
p_{41} & p_{41} & p_{42} & p_{42} \\
-e^{Lk_1}p_{11} & -e^{-Lk_1}p_{11} & -e^{Lk_2}p_{12} & -e^{-Lk_2}p_{12} \\
-e^{Lk_1}p_{21} & e^{-Lk_1}p_{21} & -e^{Lk_2}p_{22} & e^{-Lk_2}p_{22} \\
-e^{Lk_1}p_{31} & -e^{-Lk_1}p_{31} & -e^{Lk_2}p_{32} & -e^{-Lk_2}p_{32} \\
-e^{Lk_1}p_{41} & -e^{-Lk_1}p_{41} & -e^{Lk_2}p_{42} & -e^{-Lk_2}p_{42}
\end{bmatrix}$$

$$\begin{bmatrix}
p_{13} & p_{13} & p_{14} & p_{14} \\
p_{23} & -p_{23} & p_{24} & -p_{24} \\
p_{33} & p_{33} & p_{34} & p_{34} \\
p_{43} & p_{43} & p_{44} & p_{44} \\
-e^{Lk_3}p_{13} & -e^{-Lk_3}p_{13} & -e^{Lk_4}p_{14} & -e^{-Lk_4}p_{14} \\
-e^{Lk_3}p_{23} & e^{-Lk_3}p_{23} & -e^{Lk_4}p_{24} & e^{-Lk_4}p_{24} \\
-e^{Lk_3}p_{33} & -e^{-Lk_3}p_{33} & -e^{Lk_4}p_{34} & -e^{-Lk_4}p_{34} \\
-e^{Lk_3}p_{43} & -e^{-Lk_3}p_{43} & -e^{Lk_4}p_{44} & -e^{-Lk_4}p_{44}
\end{bmatrix} \tag{A2}$$

where

$$\begin{aligned}
p_{1i} &= -k_i(EA\lambda_i-\beta k_i+\varepsilon_4\mu_i) \\
p_{2i} &= EI_w k_i^3-\varepsilon_2 g_i k_i^2+\gamma\omega^2 k_i-\lambda_i(\alpha\omega^2+\beta k_i^2) \\
&\quad -\varepsilon_1\omega^2\mu_i \\
p_{3i} &= k_i(\beta\lambda_i-EI_w k_i+\varepsilon_2\mu_i) \\
p_{4i} &= -k_i(EI_\psi\mu_i+\varepsilon_2 k_i-\varepsilon_4\lambda_i)
\end{aligned} \tag{A3}$$

and λ_i and μ_i are given Eq. (18).